Article

Current Biology

Cytoskeleton Dynamics Are Necessary for Early Events of Lateral Root Initiation in *Arabidopsis*

Highlights

- Microtubule and F-actin needed for lateral root founder cell asymmetric expansion
- Auxin-dependent, microtubule-mediated feedback constrains expansion
- Cell polarization and asymmetric cell division require F-actin network
- New genetic tools for targeted perturbation of microtubules or actin

Authors

Amaya Vilches Barro, Dorothee Stöckle, Martha Thellmann, ..., Hidehiro Fukaki, Joop E.M. Vermeer, Alexis Maizel

Correspondence

joop.vermeer@botinst.uzh.ch (J.E.M.V.), alexis.maizel@cos.uni-heidelberg.de (A.M.)

In Brief

Vilches Barro et al. image, perturb, and analyze the microtubule and actin cytoskeleton during the asymmetric radial expansion of lateral root founder cells. Reorganization of the cytoskeleton is necessary for this asymmetric expansion and intertwines with auxin signaling to grant a basic polarity to these cells.

Vilches Barro et al., 2019, Current Biology *29*, 2443–2454
August 5, 2019
https://doi.org/10.1016/j.cub.2019.06.039

CellPress

Current Biology
Article

Cytoskeleton Dynamics Are Necessary for Early Events of Lateral Root Initiation in *Arabidopsis*

Amaya Vilches Barro,[1] Dorothee Stöckle,[2] Martha Thellmann,[2] Paola Ruiz-Duarte,[1] Lotte Bald,[1] Marion Louveaux,[1] Patrick von Born,[1,5] Philipp Denninger,[1,5] Tatsuaki Goh,[3,4] Hidehiro Fukaki,[4] Joop E.M. Vermeer,[2,*] and Alexis Maizel[1,6,*]
[1]Center for Organismal Studies (COS), University of Heidelberg, Im Neuenheimer Feld 230, 69120 Heidelberg, Germany
[2]Department of Plant and Microbial Biology, University of Zurich, 8008 Zurich, Switzerland
[3]Graduate School of Science and Technology, Nara Institute of Science and Technology, 8916-5 Takayama, Ikoma 630-0192, Japan
[4]Department of Biology, Graduate School of Science, Kobe University, Kobe 657-8501, Japan
[5]Present address: Max Planck Institute for Plant Breeding Research Cologne Germany (PvB) and Cell Biology and Plant Biochemistry, University of Regensburg, Regensburg (PD), Germany
[6]Lead Contact
*Correspondence: joop.vermeer@botinst.uzh.ch (J.E.M.V.), alexis.maizel@cos.uni-heidelberg.de (A.M.)
https://doi.org/10.1016/j.cub.2019.06.039

SUMMARY

How plant cells re-establish differential growth to initiate organs is poorly understood. Morphogenesis of lateral roots relies on the asymmetric cell division of initially symmetric founder cells. This division is preceded by the tightly controlled asymmetric radial expansion of these cells. The cellular mechanisms that license and ensure the coordination of these events are unknown. Here, we quantitatively analyze microtubule and F-actin dynamics during lateral root initiation. Using mutants and pharmacological and tissue-specific genetic perturbations, we show that dynamic reorganization of both microtubule and F-actin networks is necessary for the asymmetric expansion of the founder cells. This cytoskeleton remodeling intertwines with auxin signaling in the pericycle and endodermis in order for founder cells to acquire a basic polarity required for initiating lateral root development. Our results reveal the conservation of cell remodeling and polarization strategies between the *Arabidopsis* zygote and lateral root founder cells. We propose that coordinated, auxin-driven reorganization of the cytoskeleton licenses asymmetric cell growth and divisions during embryonic and post-embryonic organogenesis.

INTRODUCTION

Plants continuously form post-embryonic lateral roots (LRs) that provide anchorage and a means to forage the environment for water and nutrients. These LRs are formed from small groups of cells called founder cells, which in *Arabidopsis thaliana* are recruited from the pericycle cells adjacent to xylem cells (xylem pole pericycle [XPP]). LR morphogenesis is a self-organizing process characterized by the regular formation of cell layers and the emergence of a typical dome-shaped primordium [1–3]. LR formation invariably starts when pairs of abutting founder cells swell, their nuclei migrate toward the common cell wall, and an asymmetric, anticlinal division results in the formation of a stage I primordium (one cell layer). The following periclinal, formative divisions give rise to a new cell layer constituting a stage II primordium [2, 4–7]. Tempering with these steps by interfering with auxin signaling in the founder cells or the overlying endodermis [8–10] blocks LR initiation, whereas altering cell-wall properties [11] or the orientation of cell division planes [3] leads to formation of primordia with altered tissue organization. The specific remodeling of the founder cells preceding their division appears therefore essential for the LR to enter the right developmental track [3].

Auxin acts as a morphogenetic trigger for LRs and is required for both their initiation and growth [12–15]. During LR initiation, auxin signaling is mediated by SOLITARY ROOT (SLR)/AUX/IAA 14, and auxin response factor (ARF) proteins ARF7 and ARF19 [8, 16, 17]. Although these ARFs are necessary for founder cells to expand and enter division, a target of ARF7/19, LATERAL ORGAN BOUNDARY (LBD) 16, encoding a transcription factor, is required for their asymmetric division [18, 19]. Even though we have learned a lot about the hormonal control of LR formation [20, 21], we still lack mechanistic insights into how plants re-establish differential growth, especially in internal cell layers.

Radial expansion of LR founder cells is asymmetrical. It is more pronounced in the region where the founder cells abut, whereas it remains moderate on the opposite ends, prefiguring the future dome-shaped aspect of the LR primordium [5, 11]. This asymmetric expansion corresponds to an increase in volume, which implies generation of mechanical constraints that need to be dealt with [10]. It has been shown that such a mechanical conflict between the primordium and the overlying tissue drives the shape of the emerging LR primordium [1]. Yet, the cellular basis and mechanisms responsible for the asymmetric radial expansion of LR founder cells are unknown.

Growth anisotropy in plant cells is related to the geometry of the cell and to the mechanical properties of the cell wall, in turn mainly determined by the orientation of cellulose microfibrils [22–24]. Cortical microtubules (CMTs) guide cellulose synthase complexes [25, 26] to define a primary scaffold for the deposition of cellulose microfibrils [23]. CMTs are therefore prime

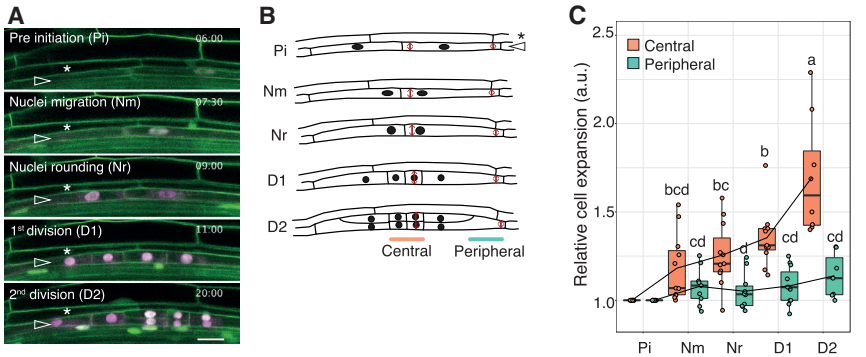

Figure 1. Asymmetric Expansion of LR Founder Cells Starts with Nuclear Migration

(A) Time-lapse image series of LR initiation visualized using *UB10pro::PIP1,4-3×GFP/GATA23pro::H2B:3×mCherry/DR5v2pro::3×YFPnls/RPS5Apro::dtTomato:NLS* (line sC111). The time (hh:min) after plants were gravistimulated and phase of development are indicated on each panel. Images were acquired every 30 min; see also Video S1. Pre-initiation, the nuclei of founder cells (open arrowhead) are positioned close to the cell center and later migrate (Nm) toward the common cell wall and round up (Nr). The cells then divide asymmetrically (D1) and undergo a second division (D2) to form a two-layered primordium. The star indicates the endodermis. Scale bar, 20 μm.

(B) Quantification of founder cell expansion in the peripheral and central domains. Boxplots of normalized width of founder cells in the central and peripheral domains during the indicated phases of LR initiation (see A). Cell width was normalized to pre-initiation (n = 11 cells quantified from stage Pi to D1 and n = 8 from Pi to D2, coming from four individual roots of three independent experiments). Comparison between samples was performed using a mixed effects model to describe the repeated measures and the Tukey method for post hoc multiple comparisons. Samples with identical letters do not significantly differ ($\alpha = 0.05$). See also Figure S1.

(C) Schematic representation of the events depicted in (A) and quantified in (B). In the central domain, cells radially expand faster and prefigure the tip of the dome-shaped primordium, whereas at the peripheral domain swelling is constrained. The open arrowhead indicates the founder cells, and the star indicates the endodermis.

determinants of plant cell growth anisotropy. The orientation of CMT arrays also influences the selection of the division plane [27]. Shortly before cell division, CMTs coalesce into a plane closely associated with the nucleus [28], forming the so-called pre-prophase band that ensures the robust positioning of the new cell wall [29]. The orientation of CMT arrays has therefore a profound influence on the direction of growth and orientation of divisions. CMT array orientation is determined by the geometry of the cell [30–32] but is also modulated by cues, such as hormones [33] and mechanics [23, 34, 35]. The F-actin cytoskeleton has been shown to affect cell shape and division through the regulation of membrane trafficking and movement of different organelles, such as the nucleus [27, 36–38]. Microtubules (MTs) and F-actin cooperate toward the polarization and directional elongation of cells [39–41]. Exemplary is the coordinated reorganization of F-actin and CMT networks driving cell outgrowth to the apical region and positioning of the nucleus for the first asymmetric division of the *Arabidopsis* zygote [40].

Despite the importance of founder cell remodeling for LR morphogenesis, there is no detailed study scrutinizing how the asymmetry in expansion is achieved, what the role of the cytoskeleton is, and how this is connected with auxin signaling. Here, we combine four-dimensional (4D) live-cell imaging, genetic and pharmacological analysis, and cell-type-specific genetic perturbation of cytoskeleton dynamics to propose a mechanistic framework for the transition from LR founder cells to a stage I primordium. We demonstrate that rearrangement of the MT and F-actin cytoskeleton and cell-wall properties contribute to the asymmetric radial expansion. We show that polar migration of the nucleus requires the F-actin network. Finally, we reveal that auxin signaling in the pericycle and the endodermis is paramount for founder cells to acquire a polarity crucial for their asymmetric radial expansion and division. This coordinated reorganization of the cytoskeleton in response to auxin signaling is required to initiate the correct developmental trajectory toward a LR primordium.

RESULTS

Asymmetric Expansion of LR Founder Cells Coincides with Nuclear Migration and MT Reorientation

Before the first asymmetric cell division (ACD) marking LR initiation, pairs of founder cells invariably expand radially and their nuclei migrate toward the common cell wall, where radial expansion is maximal [3, 4, 10, 11, 18]. To better characterize this dynamic process on a cellular scale, we performed high-resolution live imaging of *Arabidopsis* roots expressing fluorescent markers for the nucleus and the plasma membrane in which LR initiation was synchronized by gravistimulation [42] (Figure 1A; Video S1). Measurements of the cell width at the central domain, where the two founder cells are abutting, and at the peripheral domain (distal end) confirmed the asymmetric radial expansion. Founder cells expand more in the central domain than at the peripheral region (Figures 1B, 1C, and S1). Importantly, this asymmetry in radial expansion is readily quantifiable before the ACD. Indeed, during the nuclei rounding phase, cell width in the central domain increased by 22% ± 5% and stagnated at the periphery (3% ± 3%; Figure 1C; average ± SE; n = 11). This asymmetric radial expansion amplifies as the primordium progresses through its development (Figure 1C). Thus, a change in founder cell shape prior to the first division prefigures the dome-shaped appearance of the LR primordium.

CMT arrays are prime determinants of plant cell remodeling during development [43]. To visualize and quantify dynamic changes in the CMTs during the transition from founder cell to a stage I primordium, we generated *Arabidopsis* lines specifically marking MTs in the founder cells by expressing from the *GATA23* promoter [4] a fusion protein between GFP and the MICROTUBULE-ASSOCIATED PROTEIN4 (MAP4) microtubule binding domain (GFP:MBD) [44]. We observed that CMTs of non-dividing XPP cells are oriented in a spiral along the long axis of the cell (Figures 2A and S2A). In radially expanding founder cells, the CMTs were highly dynamic and progressively

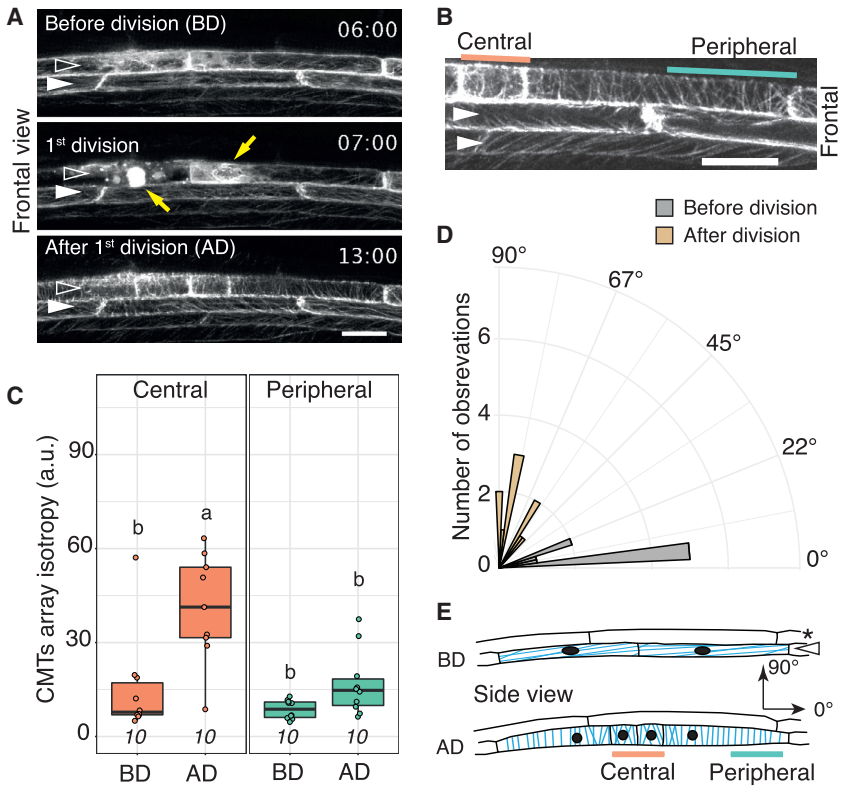

Figure 2. Reorganization of MTs in Two Domains during LR Initiation

(A) Two-photon time-lapse image series of MTs before, during, and after the first division of the founder cells visualized with *GATA23pro::GFP:MBD*. The time (hh:min) after plants were gravistimulated is indicated on each panel. Images were taken every 30 min; see also Video S2. Images show the frontal view (primordia growing toward observer) [3], and two xylem pole pericycle (XPP) cells are visible. The open arrowheads indicate the founder cells, and the filled arrowheads indicate resting (non-dividing) XPP cells. The yellow arrows indicate phragmoplast and peri-nuclear MTs. Scale bar, 20 μm. See also Figure S3.

(B) Close up of CMTs in XPP cells after the first division of the founder cell (frontal view). Orange and green lines mark the zones in which orientation and isotropy of CMTs were quantified in the central and peripheral domains, respectively. The filled arrowheads indicate resting (non-dividing) XPP cells. Scale bar, 20 μm.

(C) Quantification of CMT organization in founder cells. Boxplots of the CMT array isotropy in the central and peripheral domains of founder cells before (BD) and after the first division (AD). Ten cells coming from five individual roots of three independent experiments were measured. Comparison between samples was performed using two-way ANOVA and post hoc multiple comparisons with the Tukey test. Samples with identical letters do not significantly differ ($\alpha = 0.05$). See also Figure S3.

(D) Orientation of CMT arrays in the peripheral domain of founder cells. Histogram of mean CMT array orientation (0°–90°; see E) in the peripheral domain before and after division.

(E) Schematic side view representation of the organization of CMTs (blue) during LR initiation. Before division, CMTs in the XPP orient along the long axis of the cell (0°). After division, CMTs reorient and organize in two domains isotropic in the center and anisotropic in the periphery. The open arrowheads indicate the founder cells, and the star indicates the endodermis.

reoriented to a more transverse orientation (Figures 2A and 2B; Video S2). Interestingly, during the progression through LR initiation, the CMT arrays form distinct domains at the center and the periphery of the primordium (Figures 2B and 2C). Whereas CMTs in the central domain appeared isotropic in their organization, CMTs in the peripheral domain organized in transverse parallel arrays (Figure 2C). Although this differential CMT organization is readily apparent right after the first division and reinforces in the following hours (Video S2), it is concomitant to the asymmetric radial expansion of the founder cells, suggesting that both processes may be coordinated. To quantify this differential organization, we analyzed orientation and organization of the CMTs [45, 46] in the central and peripheral domains of the LR founder cells before and after division (Figures 2C–2E and S2A). Before division, CMTs arrange in anisotropic arrays oblique to the cell long axis. After division, CMTs in the central domain tend to arrange in isotropic arrays (Figure 2C), whereas CMTs in the peripheral domain formed ordered arrays transverse to the cell long axis (Figures 2C, 2D, and S2A). We observed similar dynamics of CMT orientation by using the MT reporter Citrine-TUA6, qualitatively corroborating our findings with the MBD marker (Figure S3A). As the GFP:MBD reporter produced high-quality images and *GATA23pro::GFP:MBD* plants did not show compromised LR formation (Figures S3B–S3D), we used this reporter to characterize CMTs in founder cells.

Taken together, as the asymmetric radial expansion of founder cells advances, CMTs become progressively more isotropic in the central area undergoing expansion and reorganize in a transversal parallel array in the area with restricted expansion.

Intact and Dynamic CMTs and Cell-Wall Integrity Are Required for Asymmetric Radial Expansion of Founder Cells

To address whether CMTs actively contribute to asymmetric radial expansion of LR founder cells, we first monitored and quantified founder cell expansion in presence of drugs that depolymerize (oryzalin) or stabilize (Taxol) CMTs. We used concentrations that affected CMTs (Figures S4A, S4D, and S4E) while not blocking cell division (Figure 3; Video S3). Twelve hours of oryzalin treatment resulted in increased radial expansion of both the central and peripheral domains, contrary to mock (DMSO) controls where only the central domain expanded (Figures 3A, 3B, and 3G). Conversely, treatment with the CMT-stabilizing drug Taxol hampered expansion of the central domain (Figures 3A, 3B, and 3G). Together, these results indicate that (1) CMT dynamics are important to license the radial expansion of the central domain and (2) that CMTs are required to constrain the radial expansion of the peripheral domain. CMTs are therefore contributing to the asymmetric radial expansion of LR founder cells.

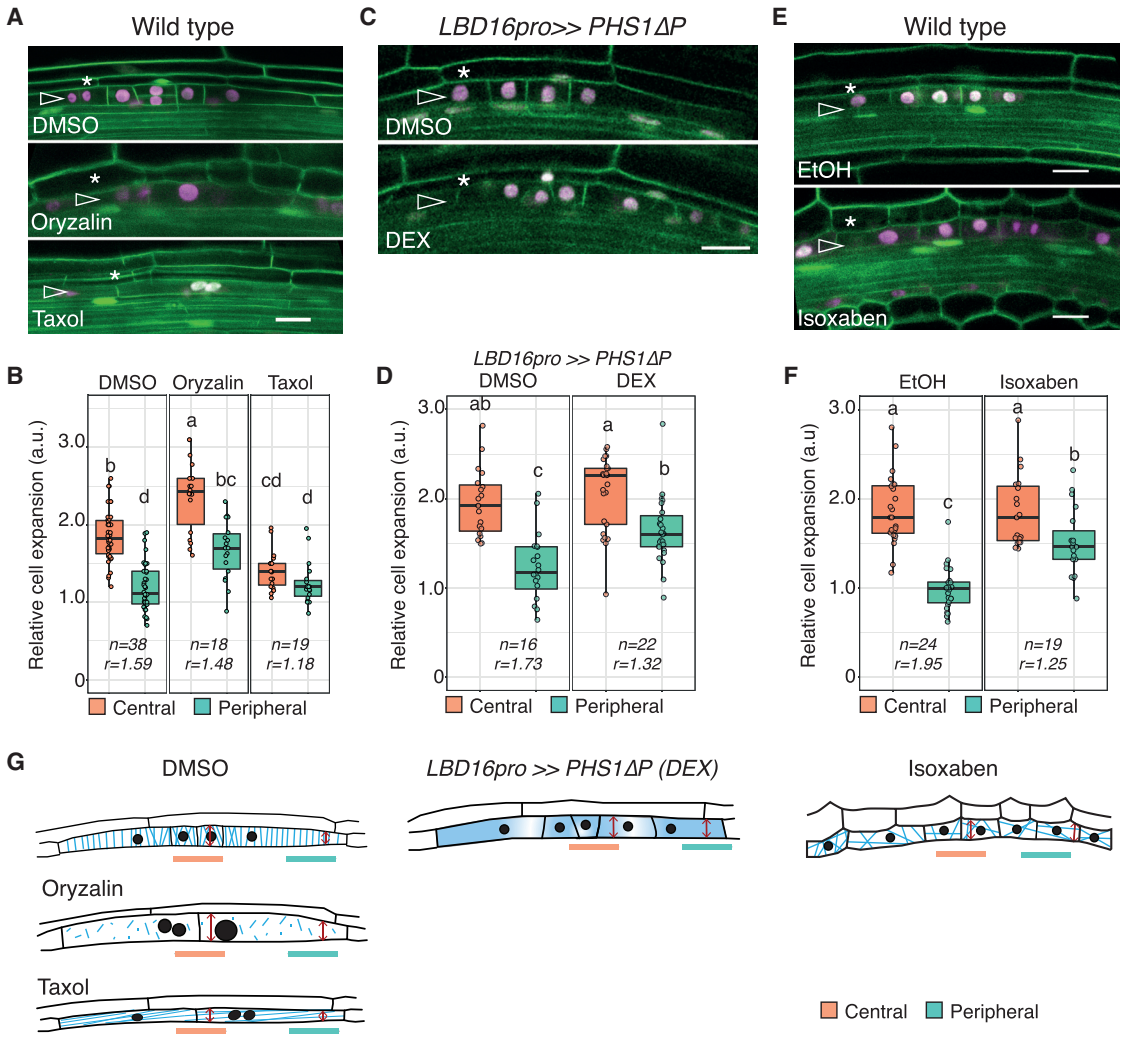

Figure 3. Alteration of MT Stability and Cell-Wall Stress Affects Asymmetric Radial Expansion of Founder Cells

(A, C, and E) Confocal sections of LR founder cells after the first division visualized with UB10pro::PIP1,4-3×GFP/GATA23pro::H2B:3×mCherry/DR5v2pro::3×YFPnls/RPS5Apro::dtTomato:NLS (line sC111). CMT dynamics was affected either by treatment with 500 nM oryzalin or 17 μM Taxol (A) or by founder-cell-specific dexamethasone-inducible expression of the CMTs depolymerizing enzyme PHS1ΔP (C). The activity of the cellulose synthase complexes was affected by 6 nM isoxaben (E). The open arrowheads indicate the founder cells, and the star indicates the endodermis. Scale bars, 20 μm. See also Figure S4 and Video S3.

(B, D, and F) Quantification of founder cell expansion. Boxplots of normalized width in the central and peripheral domains after the first cell division in response to oryzalin or Taxol (B), upon induction of PHS1ΔP in founder cells (D), or in response to isoxaben (F). Cell width was normalized to the cell width of non-dividing cells at the opposite xylem pole. The number of cells quantified is indicated below each box: (B) 38 cells from 23 individual roots from 6 independent experiments for DMSO control, 18 cells from 9 individual roots from 2 independent experiments for oryzalin, and 19 cells from 15 individual roots from 3 independent experiments for Taxol; (D) 16 cells from 10 individual roots from 2 independent experiments for DMSO control and 22 cells from 13 individual roots from 2 independent experiments for DEX; and (F) 24 cells from 8 individual roots from 3 independent experiments for ethanol control and 19 cells from 7 individual roots from 3 independent experiments. The value r indicates the ratio of expansion between the central and the peripheral domains; see also Table S2. Comparison between samples was performed by two-way ANOVA and post hoc multiple comparisons with the Tukey test. Samples with identical letters do not significantly differ ($\alpha = 0.05$).

(G) Schematic representation of the events depicted in (A) and (B) with MTs in blue. Cell width in the central and peripheral domains was measured at the position of the red arrows.

To rule out that the effects of the drug treatments on the radial expansion of the founder cells are indirect consequences of altered CMTs in the surrounding tissues, we depolymerized CMTs in a tissue-specific and inducible manner by expressing a mutated version of the atypical tubulin kinase PROPYZAMIDE-HYPERSENSITIVE 1 (PHS1) [47]. This phosphatase-inactive PHS1 (PHS1ΔP) destabilizes MTs, mimicking the effect of oryzalin. We created *Arabidopsis* lines expressing *PHS1ΔP* in the LR founder cells in response to dexamethasone (DEX) treatment (*LBD16pro>>PHS1ΔP*) and quantified radial expansion upon DEX or control (DMSO) treatments. Expression of *PHS1ΔP* in the *GATA23pro::MBD:GFP*

background verified that, upon induction, CMTs were indeed depolymerized in founder cells (Figure S4B). In response to *PHS1ΔP* induction, the peripheral domain expanded more than in control conditions (Figures 3C, 3D, and 3G), confirming that integrity of CMTs is required to constrain the expansion of the peripheral domain and allows founder cells to expand asymmetrically. Interestingly, *PHS1ΔP* induction had only marginal impact on the radial expansion in the central domain, suggesting that the "overswelling" of this region observed upon oryzalin treatment might be a consequence of altered CMTs in the overlying tissues.

CMTs serve as intracellular guides for cellulose synthase complexes and thus control the direction of cellulose deposition in the cell wall [23, 25, 26]. Our results suggest that reorganization of CMTs during LR initiation may drive deposition of cellulose defining a central cell-wall domain permissive for isotropic radial expansion (with isotropic CMTs) and a non-expanding peripheral domain (with transversal anisotropic CMTs). To challenge this model, we blocked cellulose synthesis by inhibiting cellulose synthases with isoxaben [48]. Treatment by mild doses (6 nM) of isoxaben affected the radial expansion of founder cells (Figure 3E). In presence of isoxaben, the peripheral domain expanded more than in control conditions, whereas the impact on the central region was minimal (Figure 3F). We also looked at the organization of the CMTs in founder cells upon isoxaben by imaging the *GATA23pro::GFP:MBD* (Figure S4C). Isoxaben treatment leads to isotropic organization of CMTs in all regions of the founder cells (Figures 3G and S4C). These results indicate (1) that cellulose synthesis is required to prevent the peripheral domain to radially expand and (2) that cellulose deposition provides feedback on the organization of CMTs in the peripheral domain.

Together, these results suggest that asymmetry in the radial expansion of founder cells is facilitated by constraining expansion at the peripheral domain, a process itself resulting from the feedback between CMT transversal orientation and cellulose deposition.

Perturbing Auxin Response or Founder Cell Polarity Alters MT Organization and Radial Expansion

Upon initiation, founder cells invariably undergo a first ACD. This division reflects the polarized nature of the founder cells and requires both cell-autonomous and non-cell-autonomous auxin signaling [8–10]. We asked whether the asymmetric radial expansion of founder cells and organization of CMTs are linked to auxin signaling. To test this, we needed to identify backgrounds in which XPP cells submitted to gravistimulation would divide without leading to lateral root formation. To this end, we first used plants ectopically expressing *shy2-2*, a dominant repressor of auxin signaling [49], from the endodermis-specific *CASP1* promoter (*CASP1pro::shy2-2*). Although these plants fail to initiate LRs, when submitted to gravistimulation, the XPP cells divide (2.25 ± 0.31 [mean ± SE] divisions; n = 29; Figures S5D and S5E), but these divisions are symmetric and do not lead to the formation of a primordium. We imaged *CASP1pro::shy2-2* seedlings, quantified CMT orientation (Figures 4A and S5A; Video S4), and measured the width of XPP cells as they divided symmetrically. XPP cells did not expand radially before they divided (Figure 4D), and the CMTs did not reorganize in two domains, as observed in wild type (Figure 4A). Although CMTs slightly reoriented transversally and became more isotropic, their organization resembled still the one of non-dividing cells (Figures S5B and S5C). To further test whether asymmetric radial expansion and organization of CMTs are linked to auxin signaling in the founder cells, we used the *slr1/CYCD3*^{OE} line [50]. In this line, although auxin signaling is disrupted, the overexpression of CYCLIN D3 leads to cell divisions in the XPP that are symmetric (Figure S5H) and do not lead to formation of a primordium [50]. We obtained very similar results to *CASP1pro::shy2-2*. Radial expansion was suppressed (Figure 4E), and CMT arrays did not reorganize in distinct domains (Figures 4B, S5F, and S5G; Video S4). Together, compromising auxin perception in the XPP cells or in the neighboring endodermis prevents radial expansion of XPP cells and CMT reorganization, although the cells divide. Therefore, CMT reorganization is not triggered by entry into the cell cycle.

To further test that auxin signaling actively contributes to the radial expansion of founder cells and CMT reorganization, we monitored CMT orientation in founder cells unable to polarize in response to auxin signaling. The transcription factor LBD16 is specifically expressed in the LR founder cells before the ACD [18, 19]. Expression of a genomic clone of LBD16 fused to the SUPERMAN REPRESSION DOMAIN X, *gLBD16:SRDX*, a dominant repressor of LBD-mediated gene expression, blocks the polar nuclear migration in founder cells, leading to symmetric divisions [18]. LR initiation stops after this division, and no LRs are formed [18]. We confirmed that XPP cells of *gLBD16:SRDX* plants divided symmetrically (Figure S5L). Interestingly, radial expansion occurred but was comparable in the central and peripheral domains (Figure 4F), indicating that LBDs are dispensable for the radial expansion of the founder cells but required for this expansion to be asymmetric. Quantification of CMT orientation and organization showed that CMTs reorient and form parallel arrays throughout the cell (Figures 4C, 4F, and S5I–S5K; Video S4). Together, our results show that auxin signaling is required for radial expansion and the reorganization of CMTs. The LBDs, targets of auxin signaling, are in turn required for polar migration of the founder cells nuclei and the emergence of two CMT domains licensing the asymmetric expansion.

Actin Contributes to LBD16-Dependent Polarization of LR Founder Cells

We then wondered how the polar migration of founder cell nuclei links to the asymmetric radial expansion. The movement of the nucleus in plant cells depends on an intact F-actin cytoskeleton [37, 51]. To test whether polar migration of the nucleus is required for asymmetric radial expansion and emergence of two domains of CMT organization, we treated plants with the F-actin depolymerizing drug latrunculin B (LatB). Upon LatB treatment, we did not observe any coordinated migration of nuclei in founder cells, leading to symmetric divisions (Figures 5A, 5E, S6A, and S6B) that resulted in formation of severely mis-formed LR primordia (Figure S6C; Video S5). Although we could observe radial expansion of the founder cells, it was symmetric: the peripheral domain was not constrained and expanded similarly to the central domain (Figure 5B). In these cells, CMTs organized in anisotropic transverse arrays throughout the founder cell (Figure S6D). Thus, removal of the

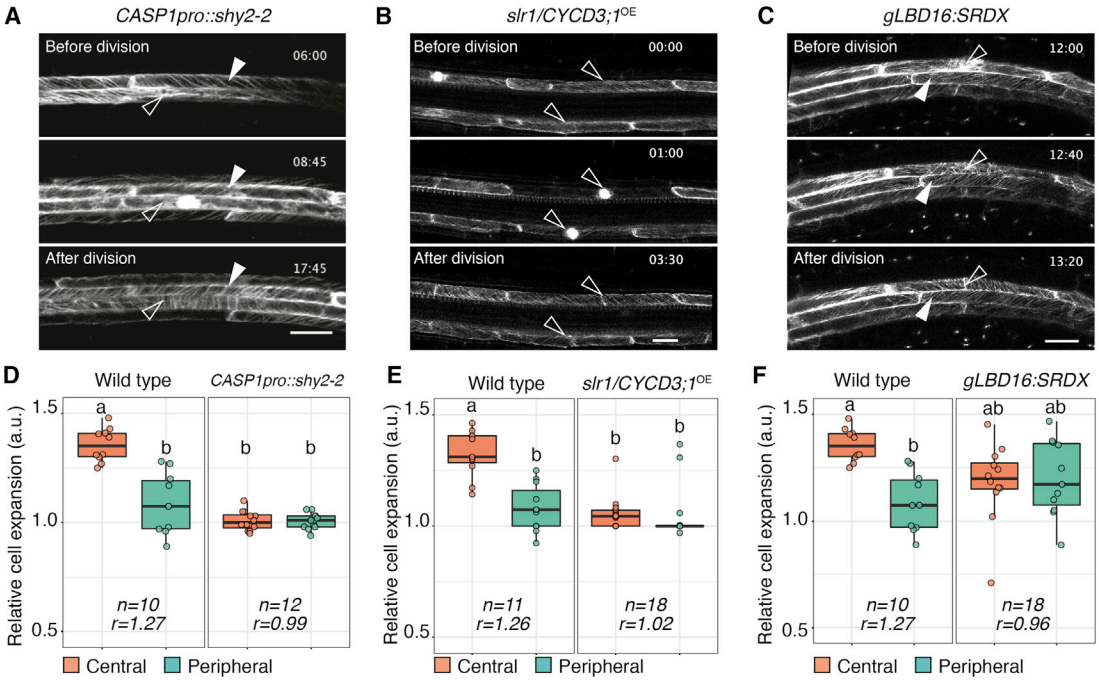

Figure 4. Asymmetric Radial Expansion of Founder Cells Requires Auxin Signaling and Cell Polarization

(A–C) Two-photon time-lapse image series of CMTs before, during, and after the first division of the founder cells visualized using *XPPpro::mVENUS:MBD* (A) or *GATA23pro::GFP:MBD* (B and C) in the indicated backgrounds. The time (hh:min) after plants were gravistimulated is indicated on each panel. Images were taken every 30 min; see also Video S4. Images show the frontal view, and two XPP cells are visible. The open arrowheads indicate the founder cells, and the filled arrowheads indicate non-dividing XPP cells. Scale bars, 20 μm.

(D–F) Quantification of founder cell expansion. Boxplots of normalized width in the central and peripheral domains after the first cell division in the indicated backgrounds are shown. Cell width was normalized to the cell width at preinitiation stage. The number of cells quantified is indicated below each box: (D) 10 cells from 8 individual roots from 4 independent experiments for wild-type control and 12 cells from 7 individual roots from 2 independent experiments for *CASP1pro::shy2-2*; (E) 11 cells from 6 individual roots from 5 independent experiments for wild-type controls and 18 cells from 6 individual roots for *slr/CYCD3;1oe*; and (F) 10 cells from 8 individual roots from 4 independent experiments for wild-type control and 18 cells from 11 individual roots for *gLBD16-SRDX* from 2 individual experiments. Wild-type samples in (D) and (F) were pooled. The value r indicates the ratio of expansion between the central and the peripheral domains; see also Table S2. Comparison between samples was performed by two-way ANOVA and post hoc multiple comparisons with the Tukey test. Samples with identical letters do not significantly differ ($\alpha = 0.05$). See also Figure S5.

F-actin network immobilizes the nuclei and leads to symmetric radial expansion and failure to establish two domains of CMT organization. To further confirm, with cell-type-specific resolution, that F-actin is required for the polar migration of the nuclei and the asymmetric radial expansion, we took advantage of the DeAct system [52]. The expression of the mono(ADP-ribosyl) transferase domain of the *Salmonella enterica* SpvB induces ADP-ribosylation of F-actin monomers, prevents formation of filamentous F-actin, and results in disassembly of all dynamic F-actin filaments [52]. We ported this system to plants (Figures S6E–S6G) and generated transgenic lines that allow inducible expression of SpvB in founder cells. Upon β-estradiol treatment, F-actin cables disappeared in founder cells (Figure S6H) and their nuclei did not migrate, resulting in symmetric divisions (Figure S6I). Comparable to LatB treatment, radial expansion was symmetric (Figures 5C–5E). Together, these results show that actin-dependent polar nuclei migration, asymmetry in radial expansion, and emergence of distinct CMT organization domains are linked.

The similitude between the phenotype observed when inhibiting LBDs activity (LBD16-SRDX) and disrupting F-actin (LatB and DeAct) led us to investigate the link between *LBD*-dependent auxin signaling and F-actin network reorganization. We first set to document F-actin dynamics in founder cells of wild-type plants expressing the second actin-binding domain of fimbrin fused to GFP (ABD2:GFP) [53] driven from the *LBD16* promoter (*LBDD16pro::GFP:ABD2*). We observed F-actin bundles along the longitudinal axis of founder cells, which disappear to form a dense peri-nuclear mesh once nuclei were positioned asymmetrically in the cell (Figures 6A and 6C; Video S6). By quantifying the organization of F-actin [45, 46], we confirmed that the isotropy of the F-actin network increased after cell division (Figure S6J). We then investigated the dynamics of F-actin in the *gLBD16:SRDX* background, where founders cells are unable to polarize in response to auxin signaling. In *gLBD16:SRDX/LBDD16pro::GFP:ABD2* roots, we observed F-actin bundles similar to wild type, although the nuclei appeared nearly immobile. Yet, we did not observe the formation of any peri-nuclear F-actin mesh in *gLBD16:SRDX/LBDD16pro::GFP:ABD2* founder cells once the cell divided. We observed bundles radiating toward the plasma membrane from the centrally positioned nucleus (Figures 6B, 6D, and S6K; Video S6). Quantification of

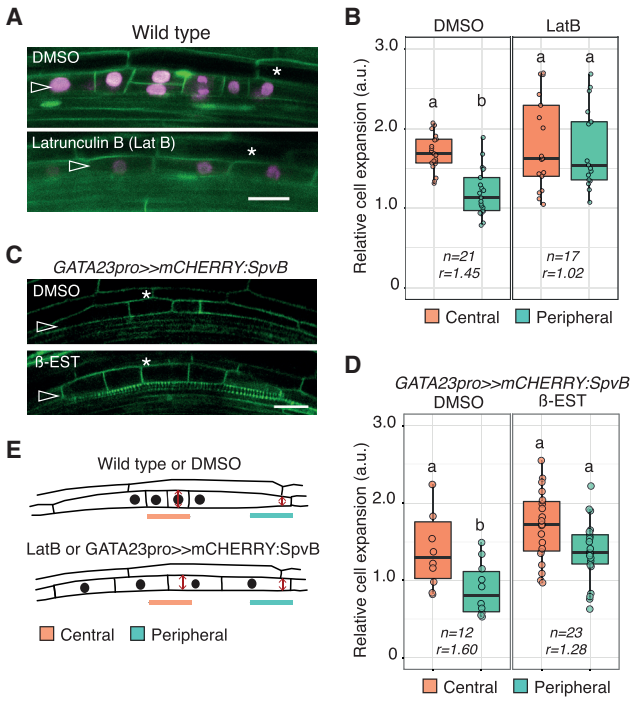

Figure 5. F-Actin Stability Is Required for Founder Cell Asymmetric Radial Expansion

(A) Confocal sections of LR founder cells after the first division visualized with *UB10pro::PIP1,4:3×GFP/GATA23pro::H2B:3×mCherry/DR5v2pro::3×YFPnls/RPS5Apro::dtTomato:NLS* (line sC111) treated as indicated. The open arrowheads indicate the founder cells, and the star indicates the endodermis. Scale bar, 20 μm.

(B) Quantification of founder cell expansion in wild type upon latrunculin B treatment (500 nM). Boxplots of normalized width in the central and peripheral domains after the first cell division upon indicated treatments are shown. Cell width was normalized to the cell width of non-dividing cells at the opposite xylem pole. The number of cells quantified is indicated below each box: 21 cells from 15 individual roots from 4 independent experiments for DMSO control and 17 cells from 8 individual roots from 3 independent experiments for latrunculin B. The value r indicates the ratio of expansion between the central and the peripheral domains; see also Table S2. Comparison between samples was performed by two-way ANOVA and post hoc multiple comparisons with the Tukey test. Samples with identical letters do not significantly differ ($\alpha = 0.05$). See also Figure S6 and Video S5.

(C) Confocal sections of *GATA23pro>>mCHERRY:SpvB* LR founder cells after the first division visualized with *WAVE131Y* upon induction by β-estradiol (β-est) or control treatment (DMSO). The open arrowheads indicate the founder cells, and the star indicates the endodermis. Scale bar, 20 μm.

(D) Quantification of founder cell expansion in *GATA23pro>>mCHERRY:SpvB*. Boxplots of normalized width in the central and peripheral domains after the first cell division upon indicated treatments are shown. Cell width was normalized to the cell width of non-dividing cells at the opposite xylem pole. The number of cells quantified is indicated below each box: 12 cells from 5 individual roots from 2 independent experiments for DMSO control and 23 cells from 7 individual roots from 2 independent experiments for β-estradiol induced. The value r indicates the ratio of expansion between the central and the peripheral domains; see also Table S2. Comparison between samples was performed by two-way ANOVA and post hoc multiple comparisons with the Tukey test. Samples with identical letters do not significantly differ ($\alpha = 0.05$). See also Figure S6.

(E) Schematic representation of the events depicted in (A) and (C). Cell width in the central and peripheral domains was measured at the position of the red arrows.

F-actin network isotropy revealed no changes in its organization (Figure S6K). Thus, LBD-mediated auxin signaling contributes to LR initiation through the coordination of F-actin dynamics, nuclear migration, and asymmetric radial expansion.

DISCUSSION

We have precisely analyzed the cellular events that precede the ACD marking the initiation of LR morphogenesis (Figure 7). We quantified the radial expansion of founder cells and observe that both founder cells coordinately and asymmetrically expand. The central domain, where the two cells are abutting, is expanding more than the distal ends, prefiguring the dome-shaped appearance of the LR primordium early on. By imaging CMTs and F-actin specifically in the pericycle and founder cells in combination with pharmacological and targeted genetic alterations, we show that F-actin and CMT reorganization contribute to the emergence of this asymmetric radial expansion. We observed that CMTs form two domains: isotropic arrays in the central domain and anisotropic transversal arrays at the periphery. Using mutants affected in the response to auxin signaling in the pericycle or in the overlying endodermis, we showed that auxin is important for triggering founder cell expansion and the reorganization of CMT arrays. Forcing cell division in the absence of auxin response is not sufficient to reorganize CMTs. On the contrary, when founder cells can respond to auxin but are unable to polarize, they radially expand albeit symmetrically. The lack of asymmetric radial expansion is intimately linked to the polar migration of the founder cell nuclei toward the common cell wall, a process requiring the F-actin network.

The asymmetric radial expansion of founder cells is paramount for LR morphogenesis. Modeling and empirical evidences have highlighted the importance of the proper execution of the first ACD for the subsequent morphogenesis of the LR [3, 11]. Here, we show that when pericycle cells are not expanding (in *CASPpro::shy2-2* and *slr/CYCD3;1*^{OE}), proper LR initiation does not proceed, although cell divisions occur. When founder cells do not polarize in response to auxin (*gLBD16:SRDX*), CMT arrays are removed (*LBD16pro>>PHS1ΔP*), or their nuclei cannot migrate (LatB treatment), they can expand radially but do it symmetrically, leading to defects in subsequent LR morphogenesis (Figures S4F and S6C). This importance of asymmetric cell expansion for the subsequent LR development bears similarities with the first division of the *Arabidopsis* zygote. In both systems, F-actin and CMTs are coordinately remodeled to ensure the polar migration of the nucleus to the cell end undergoing isotropic expansion, setting up the stage for the zygote or founder cells to undergo ACD. This ACD gives rise to a short isodiametric daughter cell, the future embryo proper or the central domain of the LR primordium, and a long daughter cell forming the embryo suspensor or the flanks of the LR primordium. Interestingly, a transcriptomic approach has revealed that a bifurcation between the transcriptional signatures of central and peripheral domains of the LRP is established very early [54], echoing the early dichotomy in cell fate observed between the daughter cells produced by the first division of the zygote [40, 55]. It is tempting to speculate that at the cell scale, embryonic and post-embryonic morphogeneses rely on similar

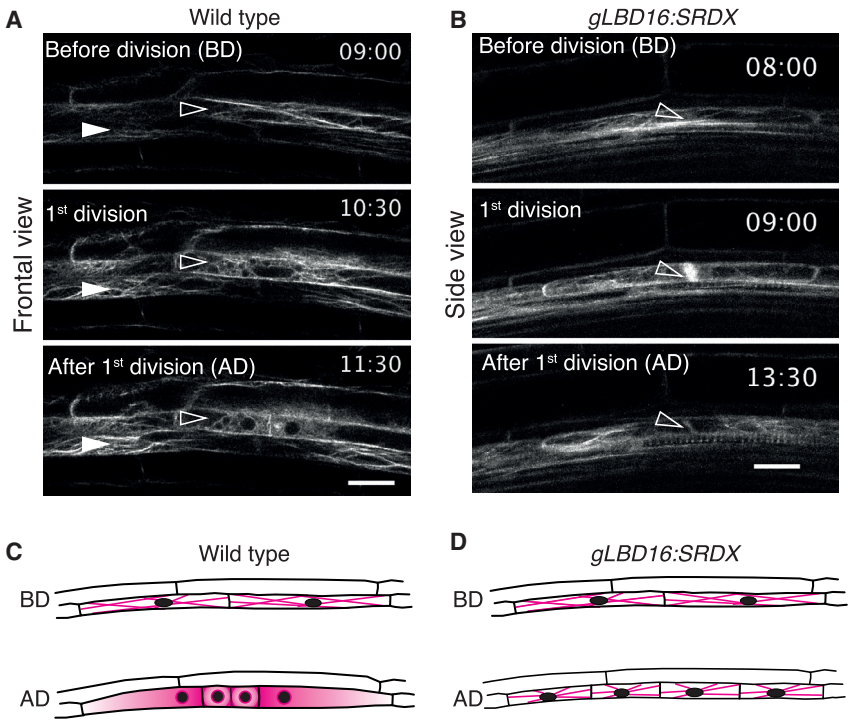

Figure 6. LBD16 Contributes to Reorganization of F-Actin Network in Founder Cells

(A and B) Two-photon time-lapse image series of F-actin before, during, and after the first division of the founder cells visualized using *LBD16pro::GFP:ABD2* in the indicated backgrounds. The time (hh:min) after plants were gravistimulated is indicated on each panel. Images were taken every 30 min; see also Video S6. Images in (A) show the frontal view, and those in (B) show the side view. The open arrowheads indicate the founder cells, and the filled arrowheads indicate non-dividing XPP cells. Scale bars, 20 μm.

(C and D) Schematic representation of the events in wild type (C) and gLBD16-SRDX (D). F-actin is represented in magenta.

mechanisms for cell remodeling and polarity acquisition. It would be interesting to follow also the vacuolar dynamics of the founder cells to see whether there is a similar dynamic remodeling as described for the zygote [56].

Beyond these parallels, LR initiation and zygote division happen in different developmental contexts, and thus their cellular environment is fundamentally different. LR initiation occurs within the parental root whose tissues actively accommodate the growth of the primordium [14, 15]. The endodermis overlying the LR founder cells actively licenses LR initiation via auxin signaling [10]. It also exerts a passive role as mechanical barrier, revealed by ablation experiments. Upon removal of the endodermis, the underlying pericycle cells increase in volume and can enter division, although these divisions are not anticlinal or asymmetric and do not lead to LR organogenesis [57]. These divisions can be partially converted to organogenic ones in presence of auxin and of dynamic CMTs [57], reminiscent of the observations reported here. Further evidence suggests a coordinated contribution of the pericycle and the endodermis toward the radial expansion of the founder cells. Oryzalin treatment affects CMTs not exclusively in the pericycle and leads to an overexpansion of the founder cells in both the central and peripheral domains compared to controls (Figure 3). On the other hand, the targeted removal of CMTs in the founder cells by *LBD16pro>>PHS1ΔP* leads to an increased radial expansion in the peripheral domain, and the central domain expansion is in magnitude comparable to the wild type. Thus, CMT integrity in the endodermis influences the magnitude of radial expansion in founder cells. It will be interesting to precisely explore the role of CMTs in the accommodation response of the endodermis.

What drives the asymmetric expansion of founder cells? Deformation of plant cells implies modification of the balance between turgor pressure and cell-wall stiffness [23]. Our results show that differential growth between the central and peripheral domains happens before the two domains of CMTs are stably established (Figures 1 and 2), suggesting CMTs are not drivers but amplifiers of an initial differential growth. This is further supported by the observation that in absence of CMTs, expansion in the peripheral domain reduces but does not abrogate the asymmetry in radial expansion. The trigger for the asymmetrical expansion is unknown, but it is tempting to speculate for geometrical reasons that it could originate from the cell wall common to the two founder cells. To our knowledge, no studies have described whether cellulose synthase genes show preferential accumulation or depletion in specific domains of founder cells during the transition into a LR primordium and its subsequent development. Alternatively, this asymmetric expansion may require the local activation of EXPANSINs, proteins that can loosen the cell wall. It was recently reported that the *Arabidopsis* EXPANSIN A1 (EXPA1) is induced by auxin and involved in the regulation of XPP cell width and the loss-of-function mutant showed aberrant cell divisions in the XPP [11, 58, 59]. One could speculate that the differential expansion in the central versus peripheral domains could result from polar secretion of EXPA1 in the central domain and/or local change in protons concentration that would locally promote the activity of EXPA1, as shown in the transition zone [60]. This mechanism could be sufficient to provide a bias toward increased deformability of the cell wall in the central domain; this bias would be reinforced by the reorientation of the CMTs guiding cellulose deposition that oppose expansion in the peripheral domain. Alternatively, local modification of the mechanical properties of the cell wall in overlying endodermis could license local expansion. The radial expansion phase correlates with highly dynamic isotropic CMT organization. We propose that such CMT dynamics are permissive for the expansion of the central domain. A shift toward isotropic CMT organization in response to auxin signaling has been previously shown to promote cell growth and organ formation in the shoot apical meristem [61]. The asymmetry in expansion originates from constraining the peripheral end to expand. Although this process requires the rearrangement of CMTs in

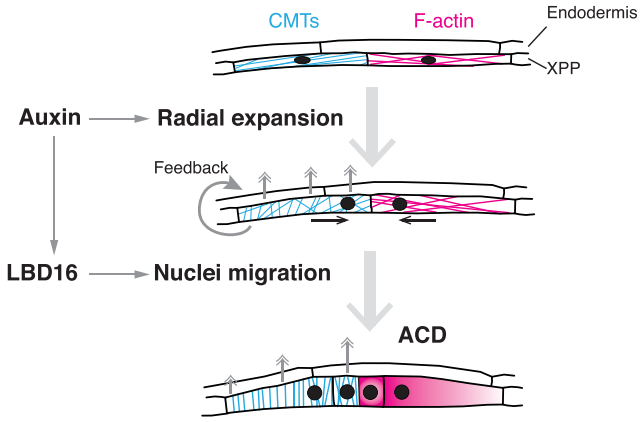

Figure 7. Schematic Representation of the Patterns and Roles of CMTs and F-Actin in LR Initiation

transversal anisotropic arrays, it is not solely driven by CMT reorganization. Uncoupling cell-wall integrity from CMTs with the isoxaben treatment revealed the existence of a feedback mechanism between the cell wall and the CMTs. We therefore propose that CMTs are part of a feedback loop amplifying the growth difference between the central and peripheral domains of the founder cells. This role of CMT dynamics in reinforcing growth heterogeneity has been involved at tissue scale in sepals and the shoot meristem [35, 62]. Local mechanical stimulation induces rapid, local reorganization of the CMTs close to the stimulated area [63]. Mechanical feedback may thus contribute to the establishment of differential growth. It is plausible that the expanding founder cell perceives the neighboring endodermis as an increased resistance to its expansion. This triggers a local reorganization of the CMTs that in turn leads to local cell-wall modification, possibly both in the founder cell and neighboring endodermis, resulting in the asymmetric expansion.

The asymmetric expansion of founder cells depends both on auxin signaling in the XPP itself but also in the endodermis. Interfering with either of these two components blocks the asymmetric swelling and results in an early arrest of LR development (Figure 4). Interestingly, in all cases, we did not observe distinct domains of CMT organization. However, in the *CASP1pro::shy2-2* and *gLBD16:SRDX* backgrounds, the CMTs of the XPP cells did rotate after executing a symmetric division, suggesting that a very specific process is blocked and not the capacity to change CMT organization, per se. In addition, in the auxin signaling mutants, we never observed coordinated ACD, as we typically found isolated single divisions in the XPP. It appears that founder cells need to acquire a basic intrinsic polarity that is dependent on auxin-mediated signaling in both the XPP and the endodermis.

Our results highlight the intimate linkage between the polarization of founder cells, CMT reorganization, and asymmetric radial expansion. By manipulating the F-actin cytoskeleton, we could phenocopy the loss of polarity observed with *gLBD16:SRDX* and showed that the F-actin network reorganization is dependent on LBD-mediated auxin signaling. It is tempting to speculate that the disruption of radial expansion and the failure of nuclei to polarly migrate observed upon F-actin disruption are causally linked. Yet, the implication of F-actin in general maintenance of cell polarity (e.g., through the dynamic of the endomembrane system) suggests that alternative mechanisms might be at play. Precise tests of the role of nuclear positioning for the asymmetric radial expansion by either micromanipulation or genetic interference with the machinery linking the nucleus to the F-actin network will be required. Therefore, it would be interesting to investigate which cytoskeleton-related genes are controlled by LBD16 or other members belonging to this family.

Here, we have developed two tools that allow to genetically interfere with the MT and F-actin cytoskeleton. To be able to control the organization of the CMTs in a cell-type-specific manner, we have introduced a genetic "oryzalin" that is based on PHS1ΔP [47]. This allowed us to specifically dissect the contribution of CMT organization in the asymmetric expansion and formation of a stage I primordium. We also generated a genetic "latrunculin," called DeAct, on the basis of genetically encoded actin-modifying proteins [52]. Expressing SpvB in plant cells efficiently disturbed the F-actin cytoskeleton. Induction of SpvB in the founder cells interfered with asymmetric expansion and nuclear migration and resulted in symmetric divisions in the XPP. These new powerful genetic tools now provide the plant community with efficient ways to functionally probe the multifaceted roles of the plant cytoskeleton during plant development.

STAR★METHODS

Detailed methods are provided in the online version of this paper and include the following:

- KEY RESOURCES TABLE
- LEAD CONTACT AND MATERIALS AVAILABILITY
- EXPERIMENTAL MODEL AND SUBJECT DETAILS
  - Plant Material and Growth Conditions
- METHOD DETAILS
  - Construction of Vectors and Transformation
  - Microscopy
  - Analysis of Radial Expansion
  - Analysis of Cytoskeleton Organization
  - Analysis of Asymmetry of Cell Division
  - Number of Cell Divisions in CASP1pro::shy2-2
- QUANTIFICATION AND STATISTICAL ANALYSIS
- DATA AND CODE AVAILABILITY

SUPPLEMENTAL INFORMATION

Supplemental Information can be found online at https://doi.org/10.1016/j.cub.2019.06.039.

ACKNOWLEDGMENTS

We thank T. Beeckmann, N. Geldner, O. Hamant, J. Lohmann, K. Schumacher, S. Vanneste, and D. Weijers for sharing published materials. We thank E. Benkova and S. Wolf for their critical reading of the manuscript. We thank the Center for Microscopy and Image Analysis of the University of Zurich for excellent technical support and assistance as well as the MAPS class of 2018 for their help with the DeAct system. Work of the Maizel lab is supported by DFG FOR2581, the Land Baden-Württemberg, the Chica und Heinz Schaller Stiftung, the CellNetworks cluster of excellence, and the Boehringer Ingelheim Foundation. Work in the Vermeer lab is supported by grants from the Swiss National Science Foundation (Schweizerischer Nationalfonds zur Förderung

der Wissenschaftlichen Forschung; PP00P3_157524 and 316030_164086) and the Netherlands Organisation for Scientific Research (Nederlandse Organisatie voor Wetenschappelijk Onderzoek; NWO 864.13.008). D.S. was supported by a travel grant from the University of Zurich to visit the A.M. lab. The ORCIDs for the authors are as follows: 0000-0001-9546-0875 (A.V.B.), 0000-0001-5786-8589 (D.S.), 0000-0001-6909-6950 (M.T.), 0000-0001-5912-0080 (P.R.-D.), 0000-0002-1794-3748 (M.L.), 0000-0003-3794-2360 (P.D.), 0000-0001-8876-5873 (J.E.M.V.), and 0000-0001-6843-1059 (A.M.).

AUTHOR CONTRIBUTIONS

A.V.B. and D.S. generated resources and performed and analyzed experiments. M.T., P.R.-D., L.B., M.L., and P.v.B. generated resources. P.D., T.G., and H.F. contributed new reagents, and J.E.M.V. and A.M. designed and analyzed the experiments and wrote the manuscript with input from all co-authors.

DECLARATION OF INTERESTS

The authors declare no competing interests.

Received: March 1, 2019
Revised: May 31, 2019
Accepted: June 12, 2019
Published: July 18, 2019

REFERENCES

1. Lucas, M., Kenobi, K., von Wangenheim, D., Voβ, U., Swarup, K., De Smet, I., Van Damme, D., Lawrence, T., Péret, B., Moscardi, E., et al. (2013). Lateral root morphogenesis is dependent on the mechanical properties of the overlaying tissues. Proc. Natl. Acad. Sci. USA *110*, 5229–5234.
2. Malamy, J.E., and Benfey, P.N. (1997). Organization and cell differentiation in lateral roots of Arabidopsis thaliana. Development *124*, 33–44.
3. von Wangenheim, D., Fangerau, J., Schmitz, A., Smith, R.S., Leitte, H., Stelzer, E.H.K., and Maizel, A. (2016). Rules and self-organizing properties of post-embryonic plant organ cell division patterns. Curr. Biol. *26*, 439–449.
4. De Rybel, B., Vassileva, V., Parizot, B., Demeulenaere, M., Grunewald, W., Audenaert, D., Van Campenhout, J., Overvoorde, P., Jansen, L., Vanneste, S., et al. (2010). A novel aux/IAA28 signaling cascade activates GATA23-dependent specification of lateral root founder cell identity. Curr. Biol. *20*, 1697–1706.
5. Dubrovsky, J.G., Rost, T.L., Colón-Carmona, A., and Doerner, P. (2001). Early primordium morphogenesis during lateral root initiation in Arabidopsis thaliana. Planta *214*, 30–36.
6. Gunning, B.E.S., Hughes, J.E., and Hardham, A.R. (1978). Formative and proliferative cell divisions, cell differentiation, and developmental changes in the meristem of Azolla roots. Planta *143*, 121–144.
7. Laskowski, M.J., Williams, M.E., Nusbaum, H.C., and Sussex, I.M. (1995). Formation of lateral root meristems is a two-stage process. Development *121*, 3303–3310.
8. Fukaki, H., Tameda, S., Masuda, H., and Tasaka, M. (2002). Lateral root formation is blocked by a gain-of-function mutation in the SOLITARY-ROOT/IAA14 gene of Arabidopsis. Plant J. *29*, 153–168.
9. Fukaki, H., Nakao, Y., Okushima, Y., Theologis, A., and Tasaka, M. (2005). Tissue-specific expression of stabilized SOLITARY-ROOT/IAA14 alters lateral root development in Arabidopsis. Plant J. *44*, 382–395.
10. Vermeer, J.E.M., von Wangenheim, D., Barberon, M., Lee, Y., Stelzer, E.H.K., Maizel, A., and Geldner, N. (2014). A spatial accommodation by neighboring cells is required for organ initiation in Arabidopsis. Science *343*, 178–183.
11. Ramakrishna, P., Ruiz Duarte, P., Rance, G.A., Schubert, M., Vordermaier, V., Vu, L.D., Murphy, E., Vilches Barro, A., Swarup, K., Moirangthem, K., et al. (2019). EXPANSIN A1-mediated radial swelling of pericycle cells positions anticlinal cell divisions during lateral root initiation. Proc. Natl. Acad. Sci. USA *116*, 8597–8602.
12. Dubrovsky, J.G., Sauer, M., Napsucialy-Mendivil, S., Ivanchenko, M.G., Friml, J., Shishkova, S., Celenza, J., and Benková, E. (2008). Auxin acts as a local morphogenetic trigger to specify lateral root founder cells. Proc. Natl. Acad. Sci. USA *105*, 8790–8794.
13. Lavenus, J., Goh, T., Roberts, I., Guyomarc'h, S., Lucas, M., De Smet, I., Fukaki, H., Beeckman, T., Bennett, M., and Laplaze, L. (2013). Lateral root development in Arabidopsis: fifty shades of auxin. Trends Plant Sci. *18*, 450–458.
14. Stoeckle, D., Thellmann, M., and Vermeer, J.E. (2018). Breakout-lateral root emergence in Arabidopsis thaliana. Curr. Opin. Plant Biol. *41*, 67–72.
15. Vilches-Barro, A., and Maizel, A. (2015). Talking through walls: mechanisms of lateral root emergence in Arabidopsis thaliana. Curr. Opin. Plant Biol. *23*, 31–38.
16. Okushima, Y., Overvoorde, P.J., Arima, K., Alonso, J.M., Chan, A., Chang, C., Ecker, J.R., Hughes, B., Lui, A., Nguyen, D., et al. (2005). Functional genomic analysis of the AUXIN RESPONSE FACTOR gene family members in Arabidopsis thaliana: unique and overlapping functions of ARF7 and ARF19. Plant Cell *17*, 444–463.
17. Wilmoth, J.C., Wang, S., Tiwari, S.B., Joshi, A.D., Hagen, G., Guilfoyle, T.J., Alonso, J.M., Ecker, J.R., and Reed, J.W. (2005). NPH4/ARF7 and ARF19 promote leaf expansion and auxin-induced lateral root formation. Plant J. *43*, 118–130.
18. Goh, T., Joi, S., Mimura, T., and Fukaki, H. (2012). The establishment of asymmetry in Arabidopsis lateral root founder cells is regulated by LBD16/ASL18 and related LBD/ASL proteins. Development *139*, 883–893.
19. Okushima, Y., Fukaki, H., Onoda, M., Theologis, A., and Tasaka, M. (2007). ARF7 and ARF19 regulate lateral root formation via direct activation of LBD/ASL genes in Arabidopsis. Plant Cell *19*, 118–130.
20. Bensmihen, S. (2015). Hormonal control of lateral root and nodule development in legumes. Plants (Basel) *4*, 523–547.
21. Fukaki, H., and Tasaka, M. (2009). Hormone interactions during lateral root formation. Plant Mol. Biol. *69*, 437–449.
22. Baskin, T.I., Meekes, H.T.H.M., Liang, B.M., and Sharp, R.E. (1999). Regulation of growth anisotropy in well-watered and water-stressed maize roots. II. Role Of cortical microtubules and cellulose microfibrils. Plant Physiol. *119*, 681–692.
23. Landrein, B., and Hamant, O. (2013). How mechanical stress controls microtubule behavior and morphogenesis in plants: history, experiments and revisited theories. Plant J. *75*, 324–338.
24. Lloyd, C.W., Clayton, L., Dawson, P.J., Doonan, J.H., Hulme, J.S., Roberts, I.N., and Wells, B. (1985). The cytoskeleton underlying side walls and cross walls in plants: molecules and macromolecular assemblies. J. Cell Sci. Suppl. *2*, 143–155.
25. Gutierrez, R., Lindeboom, J.J., Paredez, A.R., Emons, A.M.C., and Ehrhardt, D.W. (2009). Arabidopsis cortical microtubules position cellulose synthase delivery to the plasma membrane and interact with cellulose synthase trafficking compartments. Nat. Cell Biol. *11*, 797–806.
26. Paredez, A.R., Somerville, C.R., and Ehrhardt, D.W. (2006). Visualization of cellulose synthase demonstrates functional association with microtubules. Science *312*, 1491–1495.
27. Rasmussen, C.G., and Bellinger, M. (2018). An overview of plant division-plane orientation. New Phytol. *219*, 505–512.
28. Gunning, B., and Sammut, M. (1990). Rearrangements of microtubules involved in establishing cell division planes start immediately after DNA synthesis and are completed just before mitosis. Plant Cell *2*, 1273–1282.
29. Schaefer, E., Belcram, K., Uyttewaal, M., Duroc, Y., Goussot, M., Legland, D., Laruelle, E., de Tauzia-Moreau, M.-L., Pastuglia, M., and Bouchez, D. (2017). The preprophase band of microtubules controls the robustness of division orientation in plants. Science *356*, 186–189.
30. Besson, S., and Dumais, J. (2011). Universal rule for the symmetric division of plant cells. Proc. Natl. Acad. Sci. USA *108*, 6294–6299.

31. Chakrabortty, B., Willemsen, V., de Zeeuw, T., Liao, C.-Y., Weijers, D., Mulder, B., and Scheres, B. (2018). A plausible microtubule-based mechanism for cell division orientation in plant embryogenesis. Curr. Biol. *28*, 3031–3043.e2.

32. Hawkins, R.J., Tindemans, S.H., and Mulder, B.M. (2010). Model for the orientational ordering of the plant microtubule cortical array. Phys. Rev. E Stat. Nonlin. Soft Matter Phys. *82*, 011911.

33. Bouquin, T., Mattsson, O., Naested, H., Foster, R., and Mundy, J. (2003). The Arabidopsis lue1 mutant defines a katanin p60 ortholog involved in hormonal control of microtubule orientation during cell growth. J. Cell Sci. *116*, 791–801.

34. Hamant, O., Heisler, M.G., Jönsson, H., Krupinski, P., Uyttewaal, M., Bokov, P., Corson, F., Sahlin, P., Boudaoud, A., Meyerowitz, E.M., et al. (2008). Developmental patterning by mechanical signals in Arabidopsis. Science *322*, 1650–1655.

35. Uyttewaal, M., Burian, A., Alim, K., Landrein, B., Borowska-Wykręt, D., Dedieu, A., Peaucelle, A., Ludynia, M., Traas, J., Boudaoud, A., et al. (2012). Mechanical stress acts via katanin to amplify differences in growth rate between adjacent cells in Arabidopsis. Cell *149*, 439–451.

36. Szymanski, D., and Staiger, C.J. (2018). The actin cytoskeleton: functional arrays for cytoplasmic organization and cell shape control. Plant Physiol. *176*, 106–118.

37. Tamura, K., Iwabuchi, K., Fukao, Y., Kondo, M., Okamoto, K., Ueda, H., Nishimura, M., and Hara-Nishimura, I. (2013). Myosin XI-i links the nuclear membrane to the cytoskeleton to control nuclear movement and shape in Arabidopsis. Curr. Biol. *23*, 1776–1781.

38. Yang, Z. (2008). Cell polarity signaling in Arabidopsis. Annu. Rev. Cell Dev. Biol. *24*, 551–575.

39. Fu, Y., Gu, Y., Zheng, Z., Wasteneys, G., and Yang, Z. (2005). Arabidopsis interdigitating cell growth requires two antagonistic pathways with opposing action on cell morphogenesis. Cell *120*, 687–700.

40. Kimata, Y., Higaki, T., Kawashima, T., Kurihara, D., Sato, Y., Yamada, T., Hasezawa, S., Berger, F., Higashiyama, T., and Ueda, M. (2016). Cytoskeleton dynamics control the first asymmetric cell division in Arabidopsis zygote. Proc. Natl. Acad. Sci. USA *113*, 14157–14162.

41. Sampathkumar, A., Lindeboom, J.J., Debolt, S., Gutierrez, R., Ehrhardt, D.W., Ketelaar, T., and Persson, S. (2011). Live cell imaging reveals structural associations between the actin and microtubule cytoskeleton in Arabidopsis. Plant Cell *23*, 2302–2313.

42. Péret, B., Li, G., Zhao, J., Band, L.R., Voß, U., Postaire, O., Luu, D.-T., Da Ines, O., Casimiro, I., Lucas, M., et al. (2012). Auxin regulates aquaporin function to facilitate lateral root emergence. Nat. Cell Biol. *14*, 991–998.

43. Sampathkumar, A., Yan, A., Krupinski, P., and Meyerowitz, E.M. (2014). Physical forces regulate plant development and morphogenesis. Curr. Biol. *24*, R475–R483.

44. Marc, J., Granger, C.L., Brincat, J., Fisher, D.D., Kao, Th., McCubbin, A.G., and Cyr, R.J. (1998). A GFP-MAP4 reporter gene for visualizing cortical microtubule rearrangements in living epidermal cells. Plant Cell *10*, 1927–1940.

45. Boudaoud, A., Burian, A., Borowska-Wykręt, D., Uyttewaal, M., Wrzalik, R., Kwiatkowska, D., and Hamant, O. (2014). FibrilTool, an ImageJ plug-in to quantify fibrillar structures in raw microscopy images. Nat. Protoc. *9*, 457–463.

46. Louveaux, M., and Boudaoud, A. (2018). FibrilTool Batch: an automated version of the ImageJ/Fiji plugin FibrilTool, Version 1.0 (Zenodo). http://doi.org/10.5281/zenodo.2528872.

47. Fujita, S., Pytela, J., Hotta, T., Kato, T., Hamada, T., Akamatsu, R., Ishida, Y., Kutsuna, N., Hasezawa, S., Nomura, Y., et al. (2013). An atypical tubulin kinase mediates stress-induced microtubule depolymerization in Arabidopsis. Curr. Biol. *23*, 1969–1978.

48. Hamann, T., Bennett, M., Mansfield, J., and Somerville, C. (2009). Identification of cell-wall stress as a hexose-dependent and osmosensitive regulator of plant responses. Plant J. *57*, 1015–1026.

49. Tian, Q., and Reed, J.W. (1999). Control of auxin-regulated root development by the Arabidopsis thaliana SHY2/IAA3 gene. Development *126*, 711–721.

50. Vanneste, S., De Rybel, B., Beemster, G.T.S., Ljung, K., De Smet, I., Van Isterdael, G., Naudts, M., Iida, R., Gruissem, W., Tasaka, M., et al. (2005). Cell cycle progression in the pericycle is not sufficient for SOLITARY ROOT/IAA14-mediated lateral root initiation in Arabidopsis thaliana. Plant Cell *17*, 3035–3050.

51. Ketelaar, T., Faivre-Moskalenko, C., Esseling, J.J., de Ruijter, N.C.A., Grierson, C.S., Dogterom, M., and Emons, A.M.C. (2002). Positioning of nuclei in Arabidopsis root hairs: an actin-regulated process of tip growth. Plant Cell *14*, 2941–2955.

52. Harterink, M., da Silva, M.E., Will, L., Turan, J., Ibrahim, A., Lang, A.E., van Battum, E.Y., Pasterkamp, R.J., Kapitein, L.C., Kudryashov, D., et al. (2017). DeActs: genetically encoded tools for perturbing the actin cytoskeleton in single cells. Nat. Methods *14*, 479–482.

53. Sano, T., Higaki, T., Oda, Y., Hayashi, T., and Hasezawa, S. (2005). Appearance of actin microfilament 'twin peaks' in mitosis and their function in cell plate formation, as visualized in tobacco BY-2 cells expressing GFP-fimbrin. Plant J. *44*, 595–605.

54. Lavenus, J., Goh, T., Guyomarc'h, S., Hill, K., Lucas, M., Voß, U., Kenobi, K., Wilson, M.H., Farcot, E., Hagen, G., et al. (2015). Inference of the Arabidopsis lateral root gene regulatory network suggests a bifurcation mechanism that defines primordia flanking and central zones. Plant Cell *27*, 1368–1388.

55. Ueda, M., Zhang, Z., and Laux, T. (2011). Transcriptional activation of Arabidopsis axis patterning genes WOX8/9 links zygote polarity to embryo development. Dev. Cell *20*, 264–270.

56. Kimata, Y., Kato, T., Higaki, T., Kurihara, D., Yamada, T., Segami, S., Morita, M.T., Maeshima, M., Hasezawa, S., Higashiyama, T., et al. (2019). Polar vacuolar distribution is essential for accurate asymmetric division of *Arabidopsis* zygotes. Proc. Natl. Acad. Sci. USA *116*, 2338–2343.

57. Marhavý, P., Montesinos, J.C., Abuzeineh, A., Van Damme, D., Vermeer, J.E.M., Duclercq, J., Rakusová, H., Nováková, P., Friml, J., Geldner, N., and Benková, E. (2016). Targeted cell elimination reveals an auxin-guided biphasic mode of lateral root initiation. Genes Dev. *30*, 471–483.

58. Cosgrove, D.J. (2000). Loosening of plant cell walls by expansins. Nature *407*, 321–326.

59. Cosgrove, D.J. (2016). Plant cell wall extensibility: connecting plant cell growth with cell wall structure, mechanics, and the action of wall-modifying enzymes. J. Exp. Bot. *67*, 463–476.

60. Pacifici, E., Di Mambro, R., Dello Ioio, R., Costantino, P., and Sabatini, S. (2018). Acidic cell elongation drives cell differentiation in the *Arabidopsis* root. EMBO J. *37*, e99134.

61. Sassi, M., Ali, O., Boudon, F., Cloarec, G., Abad, U., Cellier, C., Chen, X., Gilles, B., Milani, P., Friml, J., et al. (2014). An auxin-mediated shift toward growth isotropy promotes organ formation at the shoot meristem in Arabidopsis. Curr. Biol. *24*, 2335–2342.

62. Hervieux, N., Dumond, M., Sapala, A., Routier-Kierzkowska, A.-L., Kierzkowski, D., Roeder, A.H.K., Smith, R.S., Boudaoud, A., and Hamant, O. (2016). A mechanical feedback restricts sepal growth and shape in Arabidopsis. Curr. Biol. *26*, 1019–1028.

63. Hardham, A.R., Takemoto, D., and White, R.G. (2008). Rapid and dynamic subcellular reorganization following mechanical stimulation of Arabidopsis epidermal cells mimics responses to fungal and oomycete attack. BMC Plant Biol. *8*, 63.

64. Liao, C.Y., Smet, W., Brunoud, G., Yoshida, S., Vernoux, T., and Weijers, D. (2015). Reporters for sensitive and quantitative measurement of auxin response. Nat. Methods *12*, 207–210, 2, 210.

65. Geldner, N., Dénervaud-Tendon, V., Hyman, D.L., Mayer, U., Stierhof, Y.-D., and Chory, J. (2009). Rapid, combinatorial analysis of membrane compartments in intact plants with a multicolor marker set. Plant J. *59*, 169–178.

66. R Core Team (2018). R: a language and environment for statistical computing (R Foundation for Statistical Computing). https://www.R-project.org/.

67. Wickham, H. (2016). ggplot2: elegant graphics for data analysis. http://ggplot2.org.

68. Wickham, H., François, R., Henry, L., and Müller, K. (2018). dplyr: a grammar of data manipulation. https://CRAN.R-project.org/package=dplyr.

69. Schindelin, J., Arganda-Carreras, I., Frise, E., Kaynig, V., Longair, M., Pietzsch, T., Preibisch, S., Rueden, C., Saalfeld, S., Schmid, B., et al. (2012). Fiji: an open-source platform for biological-image analysis. Nat. Methods *9*, 676–682.

70. Dhonukshe, P., Laxalt, A.M., Goedhart, J., Gadella, T.W.J., and Munnik, T. (2003). Phospholipase d activation correlates with microtubule reorganization in living plant cells. Plant Cell *15*, 2666–2679.

71. Andersen, T.G., Naseer, S., Ursache, R., Wybouw, B., Smet, W., De Rybel, B., Vermeer, J.E.M., and Geldner, N. (2018). Diffusible repression of cytokinin signalling produces endodermal symmetry and passage cells. Nature *555*, 529–533.

72. Alassimone, J., Naseer, S., and Geldner, N. (2010). A developmental framework for endodermal differentiation and polarity. Proc. Natl. Acad. Sci. USA *107*, 5214–5219.

73. Siligato, R., Wang, X., Yadav, S.R., Lehesranta, S., Ma, G., Ursache, R., Sevilem, I., Zhang, J., Gorte, M., Prasad, K., et al. (2016). MultiSite gateway-compatible cell type-specific gene-inducible system for plants. Plant Physiol. *170*, 627–641.

74. Nakagawa, A., Sakamoto, S., Takahashi, M., Morikawa, H., and Sakamoto, A. (2007). The RNAi-mediated silencing of xanthine dehydrogenase impairs growth and fertility and accelerates leaf senescence in transgenic Arabidopsis plants. Plant Cell Physiol. *48*, 1484–1495.

75. Lampropoulos, A., Sutikovic, Z., Wenzl, C., Maegele, I., Lohmann, J.U., and Forner, J. (2013). GreenGate—a novel, versatile, and efficient cloning system for plant transgenesis. PLoS ONE *8*, e83043.

76. Shimada, T.L., Shimada, T., and Hara-Nishimura, I. (2010). A rapid and non-destructive screenable marker, FAST, for identifying transformed seeds of Arabidopsis thaliana. Plant J. *61*, 519–528.

77. Schürholz, A.-K., López-Salmerón, V., Li, Z., Forner, J., Wenzl, C., Gaillochet, C., Augustin, S., Barro, A.V., Fuchs, M., Gebert, M., et al. (2018). A comprehensive toolkit for inducible, cell type-specific gene expression in Arabidopsis. Plant Physiol. *178*, 40–53.

78. Clough, S.J., and Bent, A.F. (1998). Floral dip: a simplified method for Agrobacterium-mediated transformation of Arabidopsis thaliana. Plant J. *16*, 735–743.

79. Moreno, A.B., Martínez de Alba, A.E., Bardou, F., Crespi, M.D., Vaucheret, H., Maizel, A., and Mallory, A.C. (2013). Cytoplasmic and nuclear quality control and turnover of single-stranded RNA modulate post-transcriptional gene silencing in plants. Nucleic Acids Res. *41*, 4699–4708.

80. Lakatos, L., Szittya, G., Silhavy, D., and Burgyán, J. (2004). Molecular mechanism of RNA silencing suppression mediated by p19 protein of tombusviruses. EMBO J. *23*, 876–884.

81. Marhavý, P., and Benková, E. (2015). Real-time analysis of lateral root organogenesis in Arabidopsis. Bio Protoc. *5*, e1446.

STAR★METHODS

KEY RESOURCES TABLE

REAGENT OR RESOURCE	SOURCE	IDENTIFIER
Chemicals, Peptides, and Recombinant Proteins		
Latrunculin B (LatB)	Sigma-Aldrich	Cat#L5288
Oryzalin	Sigma-Aldrich	Cat#36182
Taxol	Sigma-Aldrich	Cat#T7402
Isoxaben	Sigma-Aldrich	Cat#36138
β-estradiol (β-EST)	Sigma-Aldrich	Cat#E2758
Dexamethasone (DEX)	Sigma-Aldrich	Cat#D4902
Dimethyl sulfoxide (DMSO)	Honeywell	Cat#34943
Experimental Models: Organisms/Strains		
A. thaliana *DR5v2pro::3xYFP:NLS / pRPS5Apro::dtTomato:NLS*	[64]	sR251
A. thaliana *UBQ10pro::GRP:3xPIP1,4 / GATA23pro::H2B:3xmcherry*	This study	stPVB003
A. thaliana *DR5v2pro::3xYFP:NLS / pRPS5Apro::dtTomato:NLS / UBQ10pro::GRP:3xPIP1,4 / GATA23pro::H2B:3xmcherry*	This study	sC111
A. thaliana *GATA23pro::GFP:MBD*	This study	stLB033
A. thaliana *pGr179_XPPpro::mCITRINE:TUA6*	This study	stAVB07
A. thaliana *LBD16pro::LhG4:GR:6xOP:PHS1ΔP:mCherry* /sC111	This study	stPRD063
A. thaliana *LBD16pro::LhG4:GR:6xOP:PHS1ΔP:mCherry /GATA23pro::GFP:MBD*	This study	stPRD060
A. thaliana *LBD16pro::GFP:ABD2*	This study	sR407
A. thaliana *gLBD16:SRDX*	[18]	sR406
A. thaliana *gLBD16:SRDX / GATA23pro::GFP:MBD*	This study	sC101
A. thaliana *gLBD16:SRDX / LBD16pro::GFP:ABD2*	This study	sC102
A. thaliana *slr1 / CYC3;1OE*	[50]	sR450
A. thaliana *slr1 / CYC3;1OE x GATA23pro::GFP:MBD*	This study	sC142
A. thaliana *CASP1pro::shy2-2*	[10]	sR196
A. thaliana *pUB10pro::EYFP:NPSN12*	[65]	*W131Y*
A. thaliana *CASP1pro::shy2-2 / pUB10pro::EYFP:NPSN12*	[10]	sR197
A. thaliana *CASP1pro::shy2-2 / pGr179-XPPpro::mVENUS:MBD*	This study	N/A
A. thaliana *pFR-GATA23pro>>mCHERRY:SpvB*	This study	N/A

(*Continued on next page*)

Continued		
REAGENT OR RESOURCE	SOURCE	IDENTIFIER
A. thaliana *pFR-XPPpro::CITRINE:ABD2:CITRINE*	This study	N/A
A. thaliana *pFR-GATA23pro>>mCHERRY:SpvB / pFR-XPPpro::CITRINE:ABD2:CITRINE*	This study	sR533
A. thaliana *pFR-GATA23pro>>mCHERRY:SpvB /pUB10pro::EYFP:NPSN12*	This study	sR534
Deposited Data		
Cytoskeleton dynamics during lateral root initiation in *Arabidopsis thaliana*: Datasets and source code of analysis	This study	https://doi.org/10.17632/7g9dvjvswg.1
Oligonucleotides		
For primers used see Table S1		N/A
Software and Algorithms		
R	[66]	https://www.R-project.org/
ggplot2 for R	[67]	http://ggplot2.org
dplyr for R	[68]	https://CRAN.R-project.org/package = dplyr
Fiji	[69]	https://fiji.sc/
FibrilTool batch for Fiji	[45, 46]	https://github.com/marionlouveaux/FibrilTool_Batch

LEAD CONTACT AND MATERIALS AVAILABILITY

Further information and requests for resources and reagents should be directed to and will be fulfilled by the lead contact, Alexis Maizel (alexis.maizel@cos.uni-heidelberg.de).

EXPERIMENTAL MODEL AND SUBJECT DETAILS

Plant Material and Growth Conditions

The *Arabidopsis thaliana* Columbia (Col-0) ecotype was used. Seeds were surface-sterilized (Ethanol 70% and SDS 0.1% or sodium hypochlorite 5% and 0.01% Tween 20), rinsed with ethanol 99%, air-dried and stratified at 4°C for 48h. Plants were grown vertically on 1% agar supplemented with half strength Murashige-Skoog (MS) pH5.8 at 22°C under long day or constant light. For transgene induction and pharmacological treatments, stock solutions of oryzalin, taxol, latrunculin B (Lat B), dexamethasone (DEX) and β-estradiol (β-EST) were dissolved in dimethyl sulfoxide (DMSO) as indicated. The isoxaben stock solution was prepared in ethanol.

The line DR5v2pro::3xYFP:NLS / pRPS5Apro::dtTomato:NLS / UBQ10pro::GRP:3xPIP1,4 / GATA23pro::H2B:3xmcherry (sC111) was created by crossing sR251 (DR5v2pro::3xYFP:NLS / pRPS5Apro::dtTomato:NLS) with stPVB003 (UBQ10pro::GRP:3xPIP1,4 / GATA23pro::H2B:3xmcherry). Homozygosity of all markers was assessed in F3 by scoring fluorescence.

For analysis of CMTs and cell swelling in *gLBD16:SRDX*, F1 of a cross between sR406 (*gLBD16:SRDX*) and stLB033 (*GATA23pro::GFP:MBD*), were used.

For analysis of F-actin dynamics in *gLBD16:SRDX*, F1 of a cross between sR406 (*gLBD16:SRDX*) and sR407 (*LBD16pro::GFP:ABD2*), were used.

For analysis of CMTs and cell swelling in *slr1/CYC3;1*^{OE}, F1 of a cross between sR450 (*slr1/CYC3;1*^{OE}) and stLB033 (*GATA23pro::GFP:MBD*) were used.

For analysis of cell swelling in the DeAct system, *GATA23pro>>mCHERRY:SpvB* was transformed in WAVE131Y. Homozygosity of the line was determined in T3 by checking the presence of the *FastRed* cassette fluorescence.

For analysis of F-actin dynamics in the DeAct system, F1 of a cross between *pFR-GATA23pro>>mCHERRY-SpvB* and *pFR-XPPpro::CITRINE:ABD2:CITRINE* were used.

METHOD DETAILS

Construction of Vectors and Transformation

To generate *pGr179-XPPpro::mVENUS:MBD*, we cloned the region of MAP4 as described [70] using XmaI/XbaI into pGr179-OCS3′. The XPP promoter [71] was cloned into pGr179-MBD-OCS3′ using KpnI and mVENUS was cloned into pGr179-mVENUS:MBD-OCS3′

using EcorRI/XmaI. To generate *pGr179-XPPpro::mCITRINE:TUA6*, we cloned the XPP promoter in *pGr179-mCitrine:TUA6* [72] using KpnI.

To generate *GATA23pro>>mCHERRY:SpvB*, we first cloned *GATA23pro* into *p1R4-XVE* [73] using the inFusion HD cloning kit. *pEN2-SpvB-3* was constructed with Gateway cloning using BP CLONASE II (http://www.thermofisher.com) after PCR amplification of SpvB (pCMV-DeAct-SpvB; Addgene #89446). Finally, all fragments were assembled in pFR-3xGW [71] using LR CLONASE II plus [73].

To generate *XPPpro::CITRINE:ABD2:CITRINE*, we amplified CITRINE:ABD2 [72] and recombined it into pEN1-2 using BP CLONASE II. All fragments we recombined into pFR-3xGW using LR CLONASE II plus.

To generate *LBD16pro::GFP:ABD2*, a fusion gene between GFP and the second actin-binding domain (ABD2) of AtFim1 was cloned into pENTR D-TOPO as described [53] then transferred into *pGWB501:LBD16pro*, which contains thee *LBD16* promoter in front of Gateway cassette [18, 74].

The following plasmids were generated using the Green Gate system [75]. For *GATA23pro::GFP:MBD*, the following modules were combined in pGGZ001: *GATA23pro* (A), *B-dummy* (B), *GFP(A206K)* (C), *MBD* (D), *RBCS* terminator (E) and *pMAS:BastaR:tMAS* (F). The *GATA23pro* module was obtained by PCR of a 757 bp fragment corresponding to GATA23 promoter [4]. The *MBD* module was obtained by PCR of a 1254 bp fragment of *MAP4* and removal of an internal Eco31I site by silent mutation. All other modules are described in [75].

For *UBQ10pro::GFP:3xPIP1,4 / GATA23pro::H2B:3xmCHERRY*, two intermediary modules were built: pPVB005 consisting of *UB10pro* (A), *B-dummy* (B), 3x*GFP* (C), *PIP1;4* (D), *RBCS* terminator (E) FH-adaptor (F) in pGGM000 and pPVB019 consisting of *HA-adaptor*, *GATA23pro* (A), *H2B histone* (B), 3xmCherry (C), *D-dummy* (D), *UB10* terminator (E) and *pMAS:SulfR:t35S* (F) in pGGN000. Both modules were combined in pGGZ003 to generate the final vector. The *PIP1;4* module was obtained by PCR amplification of a 874 bp fragment of *PIP1;4* (At4g00430). All other modules are described in [75].

For *LBD16pro::LhG4:GR / 6xOP:PHS1ΔP:mCherry*, two intermediary modules were built: pLB040 consisting of *LBD16pro* (A), *B-dummy* (B), *LhG4:GR* (C), *D-dummy* (D), *RBCS* terminator (E) FH-adaptor (F) in pGGM000 and pLB047 consisting of *HA-adaptor*, *6xOp* (A), *B-dummy* (B), *PHS1ΔP* (C), *D-dummy* (D), *UB10* terminator (E) and *FastRed* (F) in pGGN000. Both modules were combined in pGGZ003 to generate the final vector. The *LBD16pro* module was obtained by PCR amplification of a 2157 bp fragment of *LBD16* upstream region. The *PHS1ΔP* module was obtained by PCR amplification of a 1848 bp fragment and removal of two internal Eco31I recognition by silent point mutations. The *FastRed* module was amplified from pFAST-R01 [76] and internal Eco31I removed by silent mutations. All other modules are described in [75] and [77].

For transient expression in *Nicotiana benthamiana* of the DeActs system the following plasmids were built. For *UB10-pro:3xGFP:SpvB*, the following modules were combined in pGGZ003: *UB10pro* (A), *B-dummy* (B), 3x*GFP* (C), *SpvB* (D), *RBCS* terminator (E) and *pMAS:BastaR:tMAS* (F). The *SpvB* module was obtained by PCR from pTetON -DeAct-SpvB (Addgene #89455). All other modules are described in [75].

For *UB10pro:3xGFP:GS1*, the following modules were combined in pGGZ003: *UB10pro* (A), *B-dummy* (B), 3x*GFP* (C), *GS1* (D), *RBCS* terminator (E) and *pMAS:BastaR:tMAS* (F). The *GS1* module was obtained by PCR from pTetON -DeAct-GS1(Addgene #89454). All other modules are described in [75].

For *UB10pro:LifeAct:-mRuby3*, the following modules were combined in pGGZ003: *UB10pro* (A), *B-dummy* (B), *LifeAct* (C), *mRuby3* (D), *HSP18.2* terminator (E) and *pUB10:HygR:tOCS* (F). The *LifeAct* module was obtained by PCR from pLifeAct-mTurquoise2 (Addgene ID: #36201), including a C-terminal GDPPVATS linker. The *mRuby3* module was obtained by PCR from pKanCMV-mClover3-mRuby3 (Addgene ID: #74252), including an N-Terminal GAGAGA linker. The HSP18.2 module was obtained by PCR on Col-0 gDNA (250 bp after STOP codon). All other modules are described in [75].

All oligonucleotides used for cloning are listed in Table S1.

All plasmids were sequenced prior to usage. *Arabidopsis* plants were transformed using the floral dip method [78]. At least ten individual T1 plants were analyzed and one representative homozygous line was used for experiments. Tobacco leaf infiltrations were performed as described in [79] the RNA silencing suppressor P19 was co-infiltrated [80].

Microscopy

Lateral root formation was induced by gravistimulation (180° or 90°) of seedlings at 4 or 5 days after germination (DAG) and time of gravistimulation used as reference for time lapse imaging. For imaging the seedlings were transferred to a chambered cover glass as described in [81].

Live imaging of F-actin and microtubule cytoskeleton visualized respectively with *LBD16pro::ABD2:GFP*, *GATA23pro::GFP:MBD* or *XPPpro::mCITRINE:TUA6* was performed on a Leica TCS SP5II confocal using two-photon (2P) equipped with a Spectra Physics MaiTai, DeepSee pulsed laser system for multi-photon excitation (GFP was excited at 800 nm). Images were taken with a 63x NA = 1.30 water immersion objective. For detection a hybrid photodetector operated in photon-counting mode was used (HyD) and GFP fluorescence filtered with a 495 nm-555 nm filter. Images were taken with a resolution of 1024x1024 pixels, 400 Hz speed, maximum step size (Z axis) of 1 μm and 3 to 4 times line averaging.

Live imaging of microtubule cytoskeleton visualized by *XPPpro::mVENUS:MBD* was performed with a Leica TCS SP8-MP, equipped with a resonant scanner (8 kHz) with either a 63x, NA = 1.2 water immersion objective or a 63x, NA = 1.4 oil immersion objective. Citrine and mVenus were excited with 960 nm with an insight DS+ Dual ultrafast NIR laser for multiphoton excitation. For detection, non-descanned super-sensitive photon-counting hybrid detectors (HyD), operated in photon-counting mode, were

used. EYFP/mVENUS fluorescence was filtered with a CFP/YFP filter cube (483/32 & 535/30 with SP). For more information see https://www.zmb.uzh.ch/en/Instruments-and-tools/LightMicroscopes/Multiphoton/Multiphoton-Leica-TCS-SP8-MP-(Botinst).html.

Live imaging of *UB10pro::PIP1,4:3xGFP / GATA23pro::H2B:3xmCherry / DR5v2pro::3xYFPnls / RPS5Apro::dtTomato:NLS* (line sC111) was performed with a confocal microscope Leica TCS SP8 SMD (Leica microsystems). Images were taken with a HCX PL APO 63x, NA = 1.30 water immersion objective. Images were taken with a resolution of 1024x1024 pixels, 400 Hz speed, maximum step size (Z axis) of 1μm and 3 to 4 times line averaging. Fluorescent reporters were excited with an OPSLO laser (wavelengths for GFP/YFP 480 nm and 552 nm for mCherry). For detection PMT detectors were used. GFP/YFP emission fluorescence was collected in a 493-583 nm window and 583-783 nm for mCherry and dtTomato.

Imaging of tobacco leaves was performed on a Leica SPE confocal microscope. Images were taken with an 63x, NA = 1.30 oil immersion objective at a resolution of 512x512 pixels. GFP as excited at 488 nm and mRuby at 532 nm. For detection PMT detectors were used. GFP emission fluorescence was collected in a 490-550 nm window and 620-670 nm for mRuby.

Analysis of Radial Expansion

Quantification in wild-type: sC111 seedlings were live-imaged 4h after gravistimulation every 30 min for 14 to 16 h. Five events were identified in the resulting time-lapse data: (I) preinitiation (Pi, earliest time point, no sign of initiation), (II) nuclei migration (Nm), (III) nuclei rounding (Nr) before division, (IV) first asymmetric division (D1), (V) the central cells undergo a periclinal division (D2). For each of these events, single middle plane images were selected from the z stacks and the width of the cell was measured at the central and peripheral domains with Fiji measure tool. Relative cell expansion in the central and peripheral domains was computed by dividing the cell width at each time point by the value at pre-initiation.

Quantification in mutants: for *CASP1pro::shy2-2, WAVE131Y* and *CASP1pro::shy2-2/WAVE131Y* seedlings (5 DAG) line were gravistimulated (90°) for 5 and 6 hours, respectively due to the developmental delay of initiation events between the two genotypes before imaging. Time-lapse z stacks were acquired for 14 to 16 hours every 15 to 22 min. For quantification in *slr1/CYCD3;1^{OE}, slr1/CYCD3;1^{OE}/GATA23pro:GFP:MBD* seedlings (4 DAG) were imaged immediately shootward the differentiation zone (this line being agravitropic). Time-lapse imaging data were acquired for 14 to 16 h by recording z stacks with intervals of 30 min. For quantification in *gLBD16:SRDX, gLBD16:SRDX /GATA23pro::MBD:GFP* seedlings (4 DAG) were gravistimulated (180°) for 7 h before imaging. Time-lapse z stacks were acquired for 14 to 16 hours every 40 min. In all cases, analysis of cell width was performed as described for wild-type, before and after the first division.

Quantification of cell width upon disruption of CMTs, F-actin or induction of cell wall stress. 4 DAG seedlings of the sC111 line were transferred to media containing 500 nM oryzalin, 17 μM taxol, 500 nM latrunculin B, 6nM isoxaben or DMSO or ethanol (as controls) for 3 h before gravistimulation (180°) for 12 h before imaging. For the *LBD16pro>>PHS1ΔP*, 4 DAG *LBD16pro::LhG4:GR/6xOP::PHS1ΔP:mCherry* seedlings were transferred to 10μM DEX or DMSO for 6 h before gravistimulation (180°) for 20 h before imaging. Seedlings were put back in the incubator and imaged again after 40 h. For the DeAct system, 4 DAG *GATA23pro>>mCHERRY:SpvB* seedlings were transferred to 5 μM β-EST or DMSO for 24 h before gravistimulation (180°) for 12 h before imaging. In all cases, z stacks corresponding to LR at stage I or II were acquired in the convex side of the bend and single median plane images were used to measure cell width in the central and peripheral domains using Fiji measurement tools. Similar measurements were performed on resting/non-dividing pericycle cells in the concave/opposite side of the bend and used to normalize cell width.

Analysis of Cytoskeleton Organization

Cytoskeleton organization was analyzed with the Fiji Plugin FibrilTool Batch [45, 46]. Z stacks of marker lines decorating F-actin or MTs in LR founder cells were acquired every 30 min for 14 to 16 h. First, stacks were rotated so that the longitudinal axis of cells is horizontal (0°). Then, single planes corresponding to the cell cortex before and after cell division are identified and ROIs, excluding the cell edge, are drawn where cytoskeleton is analyzed. FibrilTool returns the orientation (degrees) and quality of the cytoskeleton fibrils for each ROI (Figure S2). The quality is a measure of the anisotropy of the fibrils; a quality of 1 (highest anisotropy) corresponds to all fibrils parallel to each other. If fibrils have no directionality (lowest anisotropy), the quality will be 0. We computed the inverse of quality to represent the isotropy of the cytoskeleton before and after division. We used the absolute value of microtubule orientation (from 0° to 90°) to represent the direction of the fibrils.

Analysis of Asymmetry of Cell Division

Single median plane images of LRs at stage I were used to quantify the asymmetry of size between daughter cells after division. The length of each daughter cell was measured with Fiji measure tools and the ratio between the biggest and the smallest daughter computed.

Number of Cell Divisions in CASP1pro::shy2-2

To determine the number of cell divisions in *CASP1pro::shy2-2, CASP1pro::shy2-2/ XPPpro::mVENUS:MBD* seedlings (5 DAG) were gravistimulated (90°) for 6 h before imaging. Time-lapse data were acquired every 15 - 40 min for 14 to 16 h. We counted the total number of pericycle cells dividing in the root convex side of the bend.

QUANTIFICATION AND STATISTICAL ANALYSIS

No statistical methods were used to predetermine sample size. The experiments were not randomized and investigators were not blinded to allocation during experiments and outcome assessment. All the statistical analyses used in this study and plotting were performed in R. The methods and p-values are summarized in the figure legends.

DATA AND CODE AVAILABILITY

The accession number for the datasets and source code used for the statistical analysis reported in this paper is Mendeley Data: 10.17632/7g9dvjvswg.1.